Wolf-Rayet Stars
W.-R. Hamann, A. Sander, H. Todt, eds.
Potsdam: Univ.-Verlag, 2015
URL: http://nbn-resolving.de/urn:nbn:de:kobv:517-opus4-84268

Wolf-Rayet nebulae and the wind-interstellar medium interaction

S. J. Arthur[1]
[1]*Instituto de Radioastronomía y Astrofísica, UNAM, México*

I review our current understanding of the interaction between a Wolf-Rayet star's fast wind and the surrounding medium, and discuss to what extent the predictions of numerical simulations coincide with multiwavelength observations of Wolf-Rayet nebulae. Through a series of examples, I illustrate how changing the input physics affects the results of the numerical simulations. Finally, I discuss how numerical simulations together with multiwavelength observations of these objects allow us to unpick the previous mass-loss history of massive stars.

1 Introduction

Shells of optical nebulosity around Wolf-Rayet (WR) stars were originally identified as a class of object by Johnson & Hogg (1965). Kinematical data showed these shells to be expanding with respect to the stellar position and were interpreted in terms of a stellar wind interaction with the surrounding medium (Avedisova 1972), since the WR stars were known to have powerful stellar winds. Chu and collaborators originally classified known nebulae around WR in terms of their [OIII] and Hα morphologies (Chu 1981). The nebulae were classified as radiatively excited (essentially HII regions), ejecta nebulae or wind-blown bubbles. The ejecta nebulae are all related to WN8 stars (e.g., RCW 58), while the wind-blown bubbles are found mainly around WNE stars (e.g., S 308 and NGC 6888). A revised classification scheme (Gruendl et al. 2000) took into account the relative positions of the Hα and [OIII] emission, which can be either coincident, or in many cases the bright, clumpy Hα emission is interior to the [OIII] front.

2 Formation of Wolf-Rayet Nebulae

The general formation scenario for WR wind-blown bubbles was explained in a series of papers by García-Segura et al. (1996a,b) in terms of interacting winds. Numerical simulations were used to explore the interaction between the fast WR wind and the slow, dense wind ejected during a previous red supergiant (RSG) or luminous blue variable (LBV) evolutionary phase of the central star. Instabilities, which form at the contact discontinuity, lead to the formation of clumps and filaments composed of swept-up slow wind material that move outwards as the nebula expands. Even in these purely hydrodynamic models, useful comparisons can be made with WR nebulae such as RCW 58 and S 308. On the timescale of a few tens of thousands of years, nebulae of around 4 pc radius are formed, with expansion velocities similar to those reported from observations (50–100 km s^{-1}; Chu 1983).

Freyer et al. (2003) and Freyer et al. (2006) explored the interaction between massive stars and their environment with radiation-hydrodynamics models. Although their simulations were much lower resolution, in order to include the main sequence bubble, they found the same sorts of instabilities as García-Segura et al. (1996a,b). Furthermore, they found that the ionizing radiation emitted by the massive star is important for the energy balance of the surrounding ISM.

3 Radiation-Hydrodynamics Simulations

High-resolution, radiation-hydrodynamics simulations were carried out by Toalá & Arthur (2011) with the aim of testing 3 sets of stellar evolution models to see if the differences between the models would lead to notable observable differences in the surrounding circumstellar nebulae. They used the 40 and 60$M_\odot$ "Geneva Group" models of Meynet & Maeder (2003), both with and without stellar rotation (denoted MMROT and MM, respectively), and the corresponding STARS models (Eldridge & Tout 2004), where solar metallicity is assumed in each case. The star's radius, luminosity, surface temperature and surface gravity were used to assign a stellar wind velocity and ionizing photon rate to each time point of the evolution models using the Starburst99 code (Leitherer et al. 1999). The wind velocity and ionizing photon rate are important for the formation of the surrounding circumstellar nebulae.

The initial interstellar medium for these simulations was assumed to be uniform with a density of $n = 100$ cm^{-3} and a temperature of $T = 100$ K. In practice, WR stars begin their lives in a dense molecular cloud, often in a cluster environment. Their immediate surroundings will be affected by the ionizing radiation and stellar winds of the other cluster stars, as well as by any large scale density gradients due to the molecular cloud (Arnal & Cappa 1996). Furthermore, several WR stars are classed as runaways and have an important velocity with respect to their ambient medium (see, e.g., Reyes-Iturbide, these proceedings).

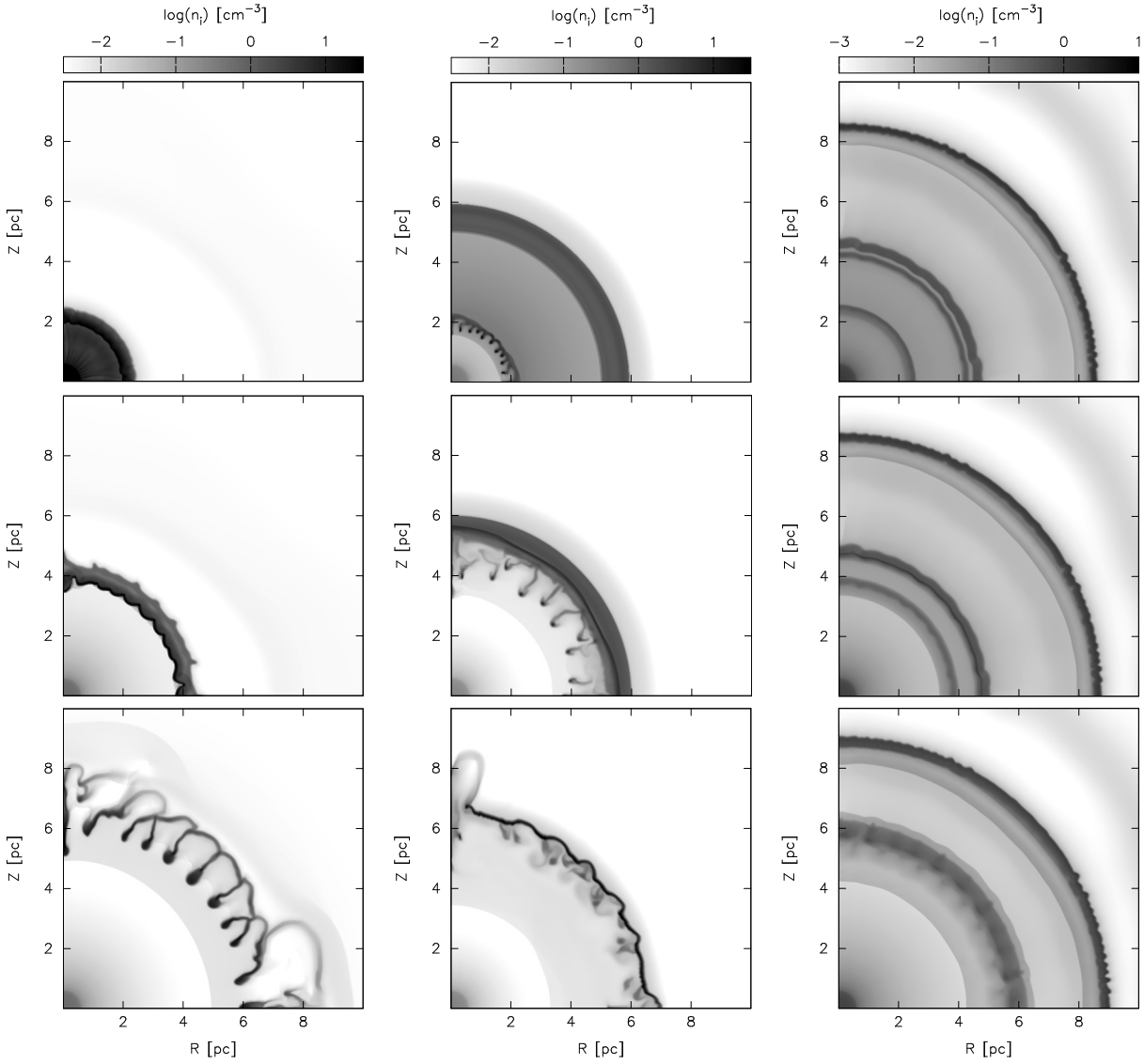

Fig. 1: Number density of ions in the r-z plane at different times after the onset of the WR stage for 3 different stellar evolution models: left - STARS (at 39800, 65900, 86000 yrs), centre - MM (at 10600, 22600, 32650 yrs), right - MMROT (at 6800, 8800, 12800 yrs). Figure adapted from Toalá & Arthur (2011). See text for details of the stellar evolution models.

Results from numerical simulations of the $40M_{\odot}$ case, corresponding to a progenitor RSG star, are shown in Figure 1. The different timescales and mass-loss rates for the period of intense mass loss immediately prior to the onset of the WR stage lead to notable differences in the wind-blown bubbles and nebulae. The stellar wind mass-loss histories of the different stellar evolution models are shown in Figure 2. These are empirical mass-loss rates, assigned according to the surface temperature, abundances and gravity of the star.

The stellar evolution models for the $40M_{\odot}$ initial mass star show that the star could evolve into either a red or yellow supergiant after leaving the main sequence. If the star becomes a yellow supergiant (YSG), the wind velocities will be of order $V_{\rm YSG} \sim 75\,{\rm km\,s^{-1}}$ (Humphreys 2010), which are higher than the velocities of red supergiant winds ($V_{\rm RSG} \sim 10\,{\rm km\,s^{-1}}$), and material that leaves the stellar surface of a YSG will get much further from the star than for a RSG in the same period of time. If the main shell of circumstellar material is dense and slow moving (the STARS models), thin-shell instabilities due to efficient cooling in the material swept up by the shock ahead of the fast wind plasma lead to the formation of clumps close to the

star, which then slowly move outwards, resulting in a small, dense, long-lived clumpy nebula. On the other hand, faster moving circumstellar material, such as is found around the models with rotation (MMROT), leads to a young, tenuous, large-diameter nebula without dense clumps.

A 3D, purely hydrodynamical, numerical study of the interaction of the WR fast wind with the surrounding circumstellar medium (CSM) formed by a progenitor RSG or LBV star was carried out by van Marle & Keppens (2012), with the assumption that the CSM was completely photoionized. They found similar results to Toalá & Arthur (2011) in that when there is a large amount of CSM material close to the star, such as occurs during a short-lived LBV stage, the resulting wind-blown bubble forms instabilities close to the star and soon after the onset of the fast wind, which leads to the sort of clumpy wind-blown bubble seen in RCW 58. On the other hand, a longer period of less intense mass loss, such as occurs during a RSG or YSG stage, leads to less fine structure. The main differences between 3D simulations and 2D simulations are that the instabilities form faster in the 3D case and so at a given time more structure is apparent in the 3D simulation results than in the 2D results.

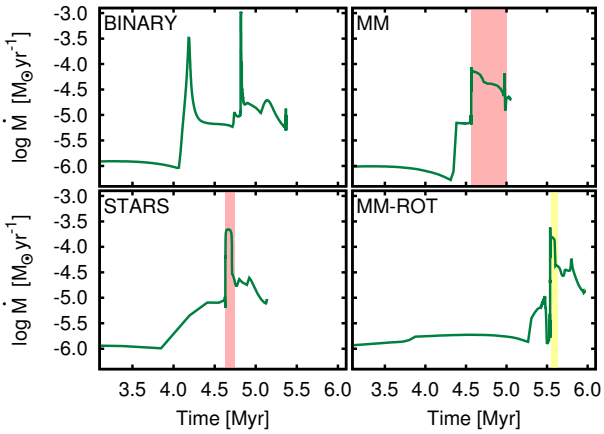

Fig. 2: Mass-loss rate against time for the STARS models and the Meynet & Maeder (2003) models with and without stellar rotation. A binary evolution model obtained from the BPASS website (Eldridge & Stanway 2009) is also included. The regions highlighted in red correspond to the range of time when the star would be considered a red supergiant, due to its low effective temperature. Similarly, the region highlighted in yellow would correspond to a yellow supergiant stage.

Numerical simulations can be used to predict the X-ray emission from the hot gas in the wind-blown bubbles (Toalá & Arthur 2011; Dwarkadas & Rosenberg 2013). The plasma immediately behind the adiabatic shock in the fast wind is too hot ($T \simeq 1.5 \times 10^7 (V_\mathrm{w}/1000\,\mathrm{km\,s^{-1}})^2$ K) and tenuous ($n \sim 0.01$ cm^{-3}) to be responsible for the observed diffuse X-ray emission, which has a typical temperature of $T_\mathrm{X} \sim 10^6$ K and density $n \sim 1$ cm^{-3} (Chu 2008). Instead, processes such as heat diffusion and thermal evaporation of the swept-up shell, or turbulent mixing layers around the clumps and filaments at the interface between the hot, shocked stellar wind and the warm (10^4 K), photoionized nebular material must be present in order to produce the substantial quantities of intermediate temperature and density gas required by the observations.

4 Toy Models

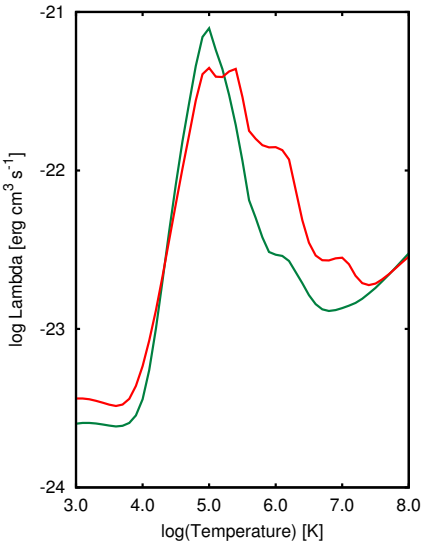

Fig. 3: Cooling rate as a function of temperature for photoionized gas with typical ISM abundances (red) and for gas with the nebular abundances of NGC 6888 (green) and the stellar photoionizing flux of WR 136.

In addition to the stellar evolution models, with their different timescales, mass-loss rates and derived fast stellar wind velocities, other factors affect the results of numerical simulations of WR wind-blown bubbles. For example, the chemical abundances in the gas heated by shock waves affect the cooling rate, which is important for the formation of clumps and filaments due to instabilities in the swept-up, radiatively cooling nebular gas. The optical nebulae around WR stars are generally found to have enhanced nitrogen and reduced oxygen abundances compared to solar values, consistent with the circumstellar material having been enriched with CNO products before being expelled from the star in a dense, slow wind (Fernández-Martín et al. 2012; Mesa-Delgado et al. 2014; Reyes-Pérez et al. 2015). The central star is the exposed stellar nucleus and thus the fast stellar wind will have different abundances on its surface to those in the nebula. In Figure 3 the cooling rates for ISM abundances and

abundances appropriate to the NGC 6888 WR nebula are shown, where the photoionizing flux of the central star WR 136 has been taken from the Potsdam Wolf-Rayet star models (Hamann & Gräfener 2004). The WR abundances lead to a higher cooling rate around 10^5 K and a lower cooling rate for million degree gas.

Another factor contributing to shaping the wind bubble could be the angular distribution of dense circumstellar material, expelled during the previous RSG, YSG or LBV stage. The bipolar nebula around the LBV Eta Carina is an obvious case, while recent ALMA observations towards the red supergiant VY Canis Majoris show that cool, dusty material is being ejected non-isotropically in directed streams (O'Gorman et al. 2015) that must persist for several tens of years in order to achieve their current extent. The density of this gas is highly inhomogeneous.

In Figure 5 snapshots from a set of numerical simulations starting from the same initial conditions but with different input physics or spatial distribution of gas are shown. The initial density distribution corresponds to a steady RSG wind with velocity 15 km s^{-1} which has expelled 15$M_\odot$ of material over 200,000 yrs. The fast wind has a wind velocity of 1600 km s^{-1} and mass-loss rate of $\dot{M}_{\rm WR} = 7 \times 10^{-5} M_\odot$ yr^{-1}. The star has an ionizing photon rate and effective temperature like that of the WNE star WR 136 and the standard model adopts abundances appropriate to the WR nebula NGC 6888. The size of the computational box is 4 pc square and the images show the number density of the ionized gas in the simulations after 18,000 yrs. Although the models without conduction look similar, some differences are apparent: changing the cooling curve (i.e., abundances) affects the thickness of the region where the shocked fast stellar wind and the swept-up CSM material mix in the turbulence around the filaments and clumps produced when the contact discontinuity corrugates due to instabilities. The thickness of the interaction region is greater for the higher metallicity simulations. The densities in the clumps themselves, which can recombine if the density becomes high enough, are also affected by the metallicity, since condensation is more rapid if the cooling rate is higher. On the other hand, thermal conduction leads to almost total evaporation of the clumps of CSM material for the set of parameters used in these toy models.

5 Non-equilibrium Shock Models

It has been postulated, for example by Moore, Hester & Scowen (2000), that cooling out of collisional ionization equilibrium behind the shock wave propagating into the dense CSM is responsible for the differences in position between the sharply defined [OIII] skin and the clumpier, interior Hα emission observed in some WR wind bubbles (those classified as types II, II and IV, e.g., S 308, RCW 58 and NGC 6888, in the scheme of Gruendl et al. (2000)). In order to test this idea, a series of models of instantaneously heated gas cooling out of equilibrium was run using the Cloudy photoionization code (Ferland et al. 2013). The requirement is that the gas reach a final photoionization equilibrium temperature of 10^4 K with a number density $n = 100$ cm^{-3}. This situation can be achieved over different time and lengthscales depending on the assumed pre-shock density and shock velocity responsible for the instantaneous heating of the gas (see Fig. 4). Slower velocity shocks cause less heating and a quick evolution to photoionization equilibrium but require a dense ambient medium. Faster shocks propagating into a more tenuous medium can reach photoionization equilibrium on lengthscales of up to 0.1 pc.

Although these models are rather unsophisticated, they do suggest that non-equilibrium cooling behind 70 – 150 km s^{-1} shock waves propagating into CSM material with densities between 0.3 and 3 cm^{-3} can explain the discrepancy in position between the [OIII] and the Hα emitting material seen in the observations. This range of velocities is consistent with the expansion velocities obtained for WR nebulae, both from radial velocities obtained from optical spectroscopy (Chu 1983) and from absorption features in IUE spectra of some WR stars, which are attributed to an expanding shell of gas around the central object (Smith, Willis & Wilson 1980).

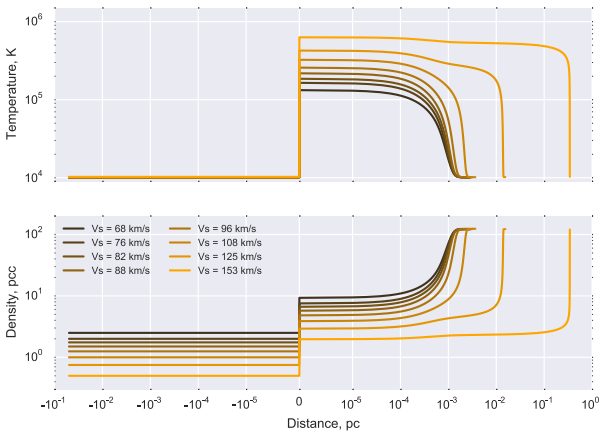

Fig. 4: Cooling regions behind shock waves for a range of shock velocities and initial densities. The requirement is to arrive at a state of photoionization equilibrium at 10^4 K and density $n = 100$ cm^{-3}.

6 Conclusions

The 2D hydrodynamic and radiation-hydrodynamic simulations developed over the past 20 years can explain WR wind bubbles in general terms. However,

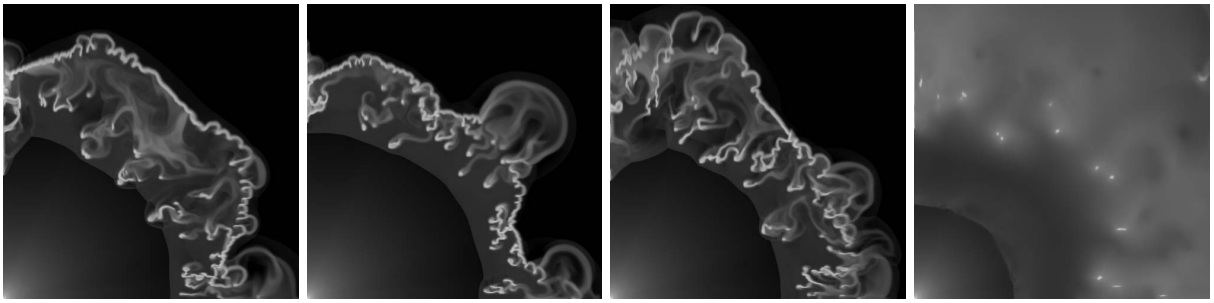

Fig. 5: Simulations starting from the same initial conditions but using different input physics: left - standard model with WR abundances; centre-left - ISM abundances; centre-right - non-spherical CSM; right - thermal conduction.

stellar evolution models are important for determining the mass loss in the RSG, YSG or LBV stage immediately prior to the onset of the fast wind and the velocity and spatial distribution of the CSM gas is important for the structure of the final nebulae.

Multiwavelength observations can constrain the models. For example, optical observations can determine the abundances, photoionization equilibrium state and cooling distances in the shocked and photoionized nebular gas. Mid-infrared observations are principally due to photon reprocessing by dust grains and can highlight the shock position and delimit the size of the wind bubble. X-ray observations are useful for determining the amount of mixing of swept-up nebular material into the hot, shocked fast wind plasma but only 3 objects have been detected so far.

The interaction of the fast wind with the environment of the WR star is responsible for a whole range of hydrodynamical phenomena, including shock waves, instabilities and mixing. A combination of high-resolution radiation-hydrodynamical simulations together with multiwavelength observations provides a laboratory for studying these processes and also for casting light on the stellar evolution process, which formed the circumstellar medium into which the fast wind expands.

The development of high-resolution 3D models with a full range of physical processes, such as radiative transfer, thermal conduction, and interaction with dust grains, would be extremely useful for disentangling the various puzzles in the interpretation of multiwavelength observations of wind-blown bubbles around WR stars.

7 Acknowledgements

SJA would like to thank Will Henney for running the non-equilibrium shock models discussed in § 5. Thanks are also due to Jesús Toalá for many discussions about numerical simulations and diffuse X-ray emission. SJA acknowledges support from UNAM through DGAPA-PAPIIT project IN101713.

References

Arnal E. M., Cappa C. E., 1996, MNRAS, 279, 788
Avedisova V. S., 1972, SvA, 15, 708
Chu Y.-H., 1981, ApJ, 249, 195
Chu Y.-H., 1983, ApJ, 269, 202
Chu Y.-H., 2008, IAUS, 250, 341
Dwarkadas V. V., Rosenberg D. L., 2013, HEDP, 9, 226
Eldridge J. J., Stanway E. R., 2009, MNRAS, 400, 1019
Eldridge, J. J., & Tout, C. A. 2004, MNRAS, 353, 87
Ferland G. J., et al., 2013, RMxAA, 49, 137
Fernández-Martín A., Martín-Gordón D., Vílchez J. M., Pérez Montero E., Riera A., Sánchez S. F., 2012, A&A, 541, A119
Freyer, T., Hensler, G., & Yorke, H. W. 2003, ApJ, 594, 888
Freyer, T., Hensler, G., & Yorke, H. W. 2006, ApJ, 638, 262
García-Segura, G., Langer, N., & Mac Low, M.-M. 1996a, A&A, 316, 133
García-Segura, G., Mac Low, M.-M., & Langer, N. 1996b, A&A, 305, 229
Gruendl, R. A., Chu, Y.-H., Dunne, B. C., & Points, S. D. 2000, AJ, 120, 2670
Hamann W.-R., Gräfener G., 2004, A&A, 427, 697
Humphreys R. M., 2010, ASPC, 425, 247
Johnson H. M., Hogg D. E., 1965, ApJ, 142, 1033
Leitherer C., et al., 1999, ApJS, 123, 3
Mesa-Delgado A., Esteban C., García-Rojas J., Reyes-Pérez J., Morisset C., Bresolin F., 2014, ApJ, 785, 100
Meynet, G., & Maeder, A. 2003, A&A, 404, 975
Moore B. D., Hester J. J., Scowen P. A., 2000, AJ, 119, 2991
O'Gorman E., et al., 2015, A&A, 573, L1
Reyes-Pérez J., Morisset C., Peña M., Mesa-Delgado A., 2015, MNRAS, 452, 1764
Smith L. J., Willis A. J., Wilson R., 1980, MNRAS, 191, 339
Toalá J. A., Arthur S. J., 2011, ApJ, 737, 100
van Marle A. J., Keppens R., 2012, A&A, 547, A3

Georges Meynet: Are there any evidences from the shape of the nebulae around WR stars that some of them are runaway stars?

Jane Arthur: Yes: in the case of a runaway star you would expect a bow shock to form ahead of the star, which forms at a stand-off distance where the ram pressure balances the shocked stellar wind pressure. We would expect the bow shock to be bright in emission lines. In the downstream direction, the stellar wind shock would be a lot further from the star and the swept-up CSM would not emit so brightly. There is evidence for such asymmetrical nebulae in objects such as M1-67 around WR 124.

Kerstin Weis: It looks like you treat the wind in the LBV phase as a steady smooth flow. In an S Dor cycle however, the wind changes $v_{\rm Wind}$ and $\dot{M}$ on a 10 to 50 yrs timescale. How would this change your results?

Jane Arthur: For simplicity, in our calculations the winds in all stages have been assumed to be isotropic. In our detailed calculations, we do take into account the time variation of the wind mass-loss rate and terminal velocity in accordance with the underlying stellar evolution models, but even so, the resolution is of order 100 years in the fastest varying stages. The effect of such a fast-varying wind as you mention is that many shells of material will be formed close to the star, however, slower shells will be overtaken by fast material coming up behind and the net result will be a shell dominated by the fastest velocity and the finer details of the mass loss will be erased.